A simplified simulation procedure for modeling an Active Magnetic Regeneration Cycle in an Electric Vehicle

Shivang Rampriyan[1,#], Bahni Ray[1]

[1]Department of Mechanical Engineering, Indian Institute of Technology, Delhi

[#]Corresponding author email: shivangrp@mech.iitd.ac.in

Abstract

An alternative to the conventional vapor-compression cycles is the Active Magnetic Refrigeration (AMR) cycle. Some materials, when magnetized or demagnetized, are observed to get heated or cooled. This is known as the Magnetocaloric Effect (MCE). Coupling other components with distinct functionalities in conjunction with the material's MCE shows promising results when employed for air-conditioning. This is particularly true for air-conditioning applications in an Electric Vehicle (EV), where the electric motor can be used to move the pistons used in the AMR cycle conveniently. Existing physical and mathematical frameworks for modeling the AMR cycle are cumbersome and computationally expensive [10]. The current study proposes a simplified numerical model for analyzing the AMR system's velocity and temperature distributions. The problem has been formulated in a way that averts the need to solve a moving boundary problem, which is one of the chief contributors to the excessive computation time. Several crucial parameters like the operating temperature span have also been calculated to assess the potential of an AMR cycle as an air-conditioning cycle in an EV.

1. Introduction

For passengers to feel hot or cold in a car cabin, the air surrounding them must be of the temperature enough to exchange just the right amount of convective heat flux for making them comfortable. To do this, researchers have done detailed analyses of the heat transfer mechanisms occurring inside the car. As new techniques were developed, resistance heating of car windows was classified as an obsolete method. Fraunhofer researchers at the IPA have made films coated with conductive carbon nanotubes (CNTs) pasted on the car doors near the passengers' arms. The nanoparticle resistance in the tubes causes the Joule effect, leading to rapid thermal comfort. Due to low film thickness, it is easy to apply when compared to conventional wire resistance heaters. The CNTs have a low specific heat capacity, meaning that most of the heat generated is dissipated [1]. On the contrary, Nissan Leaf uses seat and steering heating technologies rather than heating the entire cabin air to maintain comfortable temperatures [2].

The European Union's project called Horizon 2020 XERIC consists of new, hybrid technologies for the heating and cooling of Electric Vehicles (EVs) [3]. It is reported that the new prototype can reduce the yearly energy consumption of Heating, Ventilation, and Air-Conditioning (HVAC) systems by over 50 %. The system employs a liquid desiccant cycle for dehumidification and a conventional compressor for cooling the air. Whatever technologies we use, our motivation remains the same. We need to reduce the battery energy drawn by the HVAC systems. XERIC, therefore focuses on reducing the battery power required in HVAC. For example, the team made a compact three fluid combined membrane contactor (3F-CMC) where the membrane interface captures the air's humidity [3].

Relying heavily on localized heating concepts like seat and zone heating, the German project MAXITHERM claims to have developed HVAC systems that do not affect the EV range. They use carpets made of superior textiles that are capable of dissipating heat homogeneously. The incorporated elements could be used on the roof, steering wheel, seats, and door frame, ensuring that we can control each part of the EV almost independently of the other. Special feedback systems are also required to assess the efficacy of the prototype regularly [15]. Benoit Sicre and Patrick Baumann have studied the increase in efficiency of ventilation systems using solar panels by evaluating collector performance and heat distribution factors [4]. The same could be applied to EVs. There could also be various individual efforts and mindset transformations to take advantage of the heat generated while charging the car, for example, using the waste heat to heat drinking water.

A different set of problems arises when focusing on air-conditioning in electric vehicles. Since heat is a low-grade form of energy, it might be cheaply available or produced. However, driving a refrigeration cycle requires external work, which is usually expensive. This problem has caused the researches in air-conditioning of Battery EVs (BEVs) to progress slower than their heating counterparts. The current work introduces and develops one such cooling technology, called magnetic refrigeration. This not-in-kind technique exploits the entropy transformation property of magnetic materials and uses them to produce cooling effects in the system that may further be used to develop an air-conditioning cycle. There are many prevalent technologies for magnetic refrigeration [5–7], out of which we pick up the one called Active Magnetic Regeneration (AMR), propose a simplified model that is computationally frugal, and calculate some of its performance parameters. Simultaneously, the AMR technology is introduced in greater depth for an efficient understanding of the processes involved.

2. Model Development

We have developed a 2D numerical model for explaining the heat transfer and fluid flow characteristics of an AMR cycle. Petersen [8] has described a comprehensive mathematical model for obtaining useful performance parameters of an AMR system. The model accounts for the associated physical processes as well as the losses experienced by the system. Our work uses a model geometry similar to that given in [8]. We have chosen to study a parallel-plate regenerator that is observed to give a better performance compared to a packed bed AMR [9]. It is also easier to control the regenerator's shape and dimensions to improve the module's heat transfer. The model provided in [8] is quite challenging to implement with limited computational resources. It is also mentioned in [8] that to achieve a steady-state temperature in the cold heat exchanger (CHEX), the software required a solution time of 53 hours, implying that the model is inherently tedious. Therefore, several simplifications have been made to the modeling strategies used in [8] to reduce the computational costs, as mentioned in the following sections.

2.1 Functionality and modeling simplifications

The AMR cycle can be characterized by four distinct sequential processes. As shown in Fig. 1(a), the first process is the adiabatic magnetization of the Gadolinium refrigerant (henceforth GdR). It is assumed that the MCE starts as soon as the GdR is subjected to an external magnetic field and continues until the maximum value of the adiabatic temperature change is attained. Heat transfer from the GdR to the fluid is initiated as soon as the former's temperature exceeds the latter. The fluid is associated with heat transfer to and from the GdR, and it may be aptly termed as the system's heat transfer fluid. The concurrent transient effects of the temperature
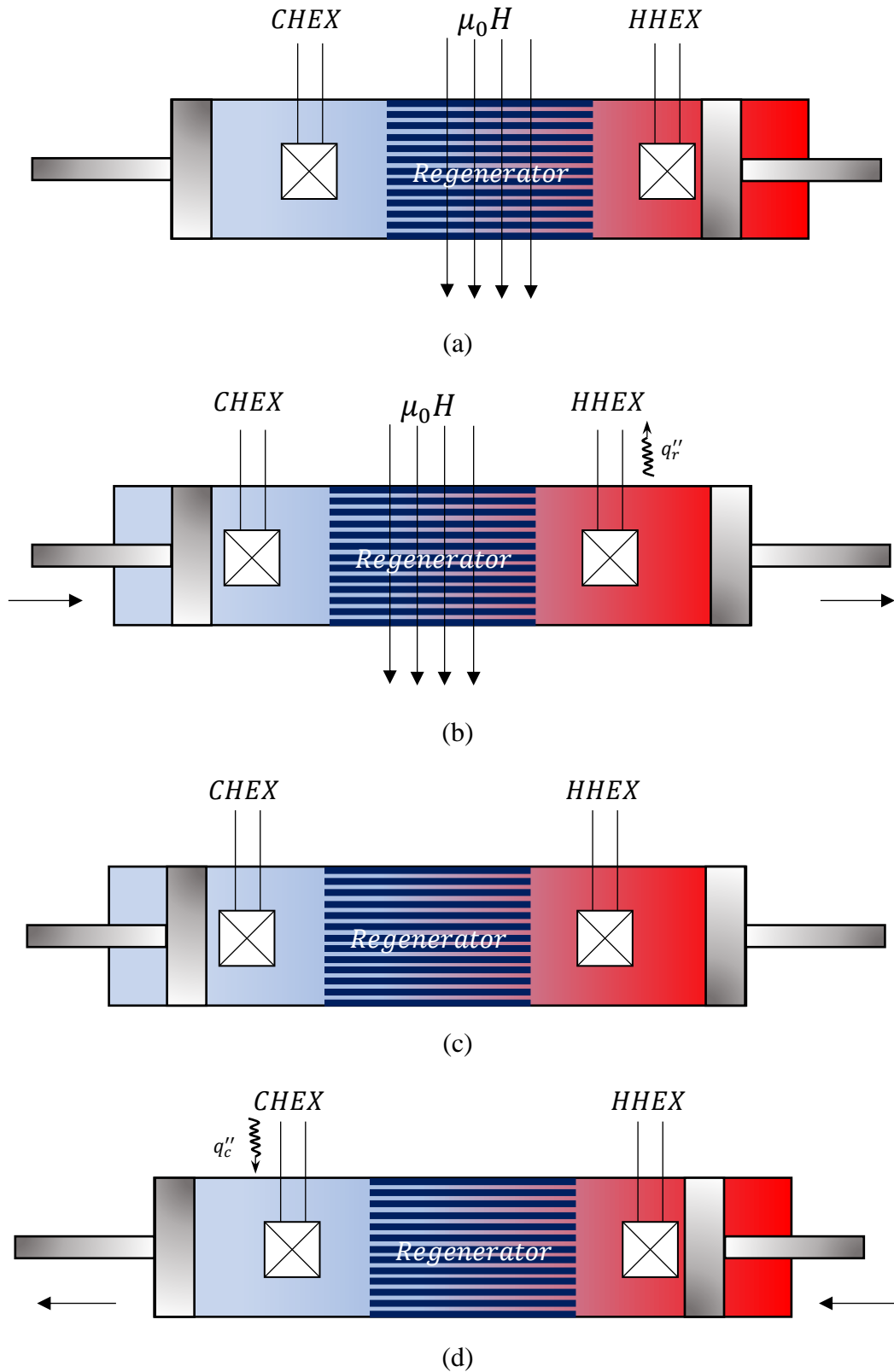
Fig. 1. Sequential illustration of the processes involved in the AMR cycle associated with the current model. (a) Adiabatic magnetization of the GdR with no force on the pistons, (b) The cold blow with force on the CHEX piston, q_r'' is the heat rejected to the surroundings (c) Adiabatic demagnetization of the GdR with relaxed pistons, (d) Hot blow with a force on the HHEX piston, q_c'' is the cooling load absorbed.

rise in the GdR, heat transfer to the fluid, and the fluid's temperature increase are difficult to model numerically. Therefore, we assume that the magnetization process of the AMR is instantaneous and the heat transfer to the fluid starts only after the magnetization is completed.

The second process concerns the cold blow. Due to the absorption of heat from the regenerator, the heat transfer fluid near it gets hotter. The piston at the left end is pushed towards the right, forcing the fluid in CHEX to displace the hot fluid into the hot heat exchanger (HHEX), which finally rejects the carried heat into the surroundings. In effect, it can be said that in an AMR cycle, the heat transfer fluid acts as a thermal energy carrier. Since the fluid displaces the hot fluid from the CHEX, this process is called a "cold blow". Fig. 1(b) illustrates this phenomenon.

Note that at the end of the second process, the GdR stays magnetized. As with most other Magnetocaloric Materials (MCMs), the internal energy of Gd increases when it is magnetized and decreases when demagnetized. The third process involves the demagnetization of the GdR, thereby lowering its temperature due to its MCE. When the temperature of the GdR decreases below the temperature of the fluid in its contact, the heat transfer fluid loses heat which simultaneously heats the GdR, further cooling the section of the fluid near the GdR. Similar to the first process, we assume that heat transfer between the GdR and the fluid starts only when the GdR is completely demagnetized. To further simplify the modeling procedure, hysteresis is neglected, which might be a flawed presumption for some materials, but works quite well in the cased of a GdR [7,10,11].

The fourth and final process in an AMR cycle may be termed a "hot blow". The piston on the HHEX side is pushed towards the CHEX, thereby drawing the heat transfer fluid from the HHEX. This extra fluid then displaces the cooled fluid section (as mentioned in the third process), driving it into the CHEX. The cooled fluid then absorbs the cooling load, thus cooling the target area. In this process, the fluid contained in the CHEX gets hotter than it was at the end of the third process. Fig. 1(d) illustrates the fourth process. The four processes in the sequence presented above constitute an AMR cycle.

Given the short stroke-times of the pistons (see Section *2.2* on operating parameters), the CHEX may not reach a steady-state temperature in a single cycle. Accordingly, multiple cycles may be needed for this purpose. In the work by Petersen [8], 600 cycles were required for the CHEX temperature to reach a steady-state value. Simulating all the cycles was reported to require a computation time of 53 hours [8]. Since such behemoth calculations are impossible to perform on a low-spec workstation, we will start our modeling at a time when 600 cycles have already passed, and the CHEX has achieved an isothermal state with a Dirichlet temperature boundary condition.

2.2 Geometry and operating parameters

As mentioned in [8], the original system was a cluster of parallel-plate channels arranged inside a hollow cylindrical tubing. The model was modified and simplified to suit our requirements. Fig. 2 shows a schematic for the reciprocating parallel-plate AMR model considered in this study. The insulating gaps are non-interacting components, so they do not require the assignment of any material. The length is measured along the x-axis, while the height is measured along the y-axis. We assume identical plates on either side of the heat transfer fluid, which creates a symmetry boundary condition in the fluid channel. This boundary condition ensures that we need to consider only half of the channel, thereby reducing redundant solution steps. The CHEX and HHEX are modeled as isothermal rectangular slabs. Table 1 lists the dimensions and the materials used in the numerical model.
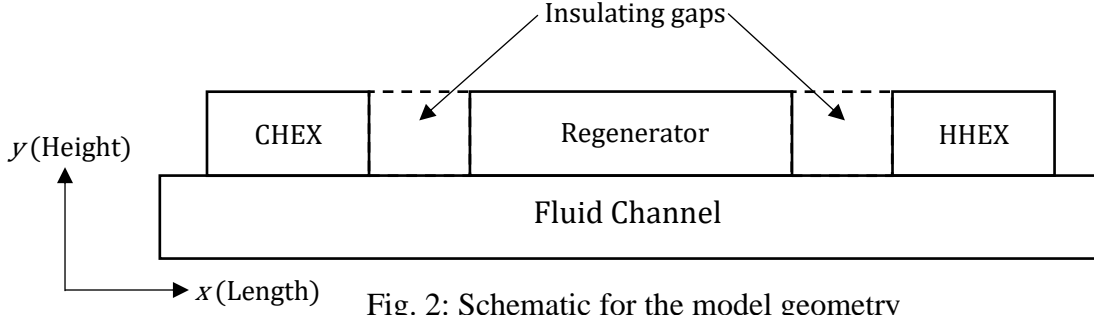
Fig. 2: Schematic for the model geometry

Table 1: Geometry of the model and materials used.

Component	Material	Length (mm)	Height (mm)
Regenerator	Gadolinium	50	0.5
Heat Exchangers	Copper	20	0.5
Fluid Channel	Water	160	0.5
Insulating Gaps	Not modeled	10	0.5

Table 2: Operating parameters used in the model

Operating parameter	Value
Stroke length	2 cm
τ_1 and τ_3 (Times allowed for heat transfer between GdR and fluid)	2 s
τ_s (Settling time for uniformization of temperature in GdR)	0.3 s
τ_2 and τ_4 (Times for executing the hot and cold blows)	1 s
Total cycle time ($\tau_1 + \tau_2 + \tau_s + \tau_3 + \tau_4$)	6.3 s
$\mu_0 H$ (Magnetization produced due to external magnetic field)	1 T

2D temperature variations have been considered in the regenerator, thereby overcoming the dimensional limitations of the 1D models proposed in [5,12]. The insulating gaps between the heat exchangers and the refrigerant enable us to approximate the fluid flow as a flow through an infinite channel. Since the pistons are considered insulating, we have not modeled them in the heat transfer study. However, the average piston velocity has been assumed to be equal to the inlet velocity of the heat transfer fluid, thereby incorporating the effect of piston movement on the fluid flow in the system. The system, therefore, depends substantially on the velocity of the pistons. From [8], we are aware of the stroke length of the pistons as well as the AMR cycle times. Assuming that the pistons move with constant velocities, dividing the stroke length by the time taken by the pistons to complete the stroke gives us the piston velocity, and therefore the inlet velocity of the heat transfer fluid. The operating parameters related to the AMR cycle are given in Table 2 [8].

2.3 Governing equations and boundary conditions

The hydrodynamics involved with the flow of the heat transfer fluid through the channel can be solved using the continuity and Navier-Stokes equations. The temperature distribution in the system can be described by the advection-diffusion equations applied to individual domains. Based on the sequence of the functioning of the AMR cycle, the modeling procedure undertaken in this study is divided into the following three steps:

2.3.1 Step 1—Velocity distribution of the heat transfer fluid

This is the initial step of the numerical procedure. In this step, we assume the fluid properties to be independent of the fluid's temperature distribution. This simplifying assumption decouples the hydrodynamic equations from the energy equation, which further implies that once we obtain the fluid's velocity distribution, it stays the same throughout the simulation. The velocity field in the channel may be obtained by the simultaneous solution of the mass-continuity (Eq. (1)) and Navier-Stokes (Eqs. (2) and (3)) equations as follows:

$$\rho \boldsymbol{\nabla} \cdot \boldsymbol{u} = 0 \tag{1}$$

$$\rho (\boldsymbol{u} \cdot \boldsymbol{\nabla}) \boldsymbol{u} = \boldsymbol{\nabla} \cdot (-P\mathbf{I} + 2\mu\mathbf{K}) + \mathbf{F} \tag{2}$$

$$\mathbf{K} = \frac{1}{2} (\boldsymbol{\nabla} \boldsymbol{u} + (\boldsymbol{\nabla} \boldsymbol{u})^T) \tag{3}$$

where ρ is the density of the fluid, $\boldsymbol{u}$ represents the velocity field in the channel, P is the pressure, μ is the dynamic viscosity, $\mathbf{K}$ is the strain rate tensor, and $\mathbf{F}$ is the body force term.

Since we are considering a 2D model, there is no body force due to gravity. Therefore, Eq. (2) simplifies to:

$$\rho (\boldsymbol{u} \cdot \boldsymbol{\nabla}) \boldsymbol{u} = \boldsymbol{\nabla} \cdot (-P\mathbf{I} + 2\mu\mathbf{K}) \tag{4}$$

The boundary conditions applicable to a general channel flow problem will work here as well. The interface of the channel and the GdR is subject to the no-slip and no-fluid separation boundary conditions. Collectively,

$$\boldsymbol{u} = \mathbf{0} \tag{5}$$

Since we consider a half-channel in our study, the center-line is also the symmetry line, and a symmetry boundary condition is implemented in COMSOL. The problem under consideration involves a movable piston, and a moving-boundary solution might be favorable to implement here. However, this significantly increases the computational costs [7,8]. Therefore, we have devised a modeling methodology that averts the need to use a moving-boundary formulation. We have implemented this by restricting the piston stroke-times to values such that the heated section of the fluid does not exit the channel, which further entails that the fluid behavior in the channel is roughly similar to that of a general channel flow. Fig. 3 illustrates all boundary conditions required for solving the flow regime in the channel.

2.3.2 Step 2—Modeling the magnetization and cold blow

The MCE occurs as soon as the GdR is magnetized [6]. This model makes a simplifying assumption that the heat transfer between the GdR and the fluid channel only starts after the GdR is completely magnetized. Assuming an adiabatic magnetization, it is possible to obtain the temperature of the GdR immediately after magnetization as:

$$T = T_i + \Delta T_{\text{ad}}^{mag} (T_i, H_0) \tag{6}$$

where T is the local temperature of the GdR after magnetization, T_i is the temperature of the GdR at the previous step, and $\Delta T_{\text{ad}}^{mag} (T_i, H_0)$ is the adiabatic temperature change when the GdR is magnetized by an external magnetic field that is increased from zero to H_0 in a single step.

It is also assumed that the magnetization due to H_0 produces a spatially independent magnetization in the GdR. To solve for the temperature distribution in the system after magnetization, the advection-diffusion equations are used for the solid GdR (Eqs. (7), (8)) and the heat transfer fluid (Eq. (9)) domains:

$$\boldsymbol{\nabla} \cdot \boldsymbol{q} = 0 \tag{7}$$
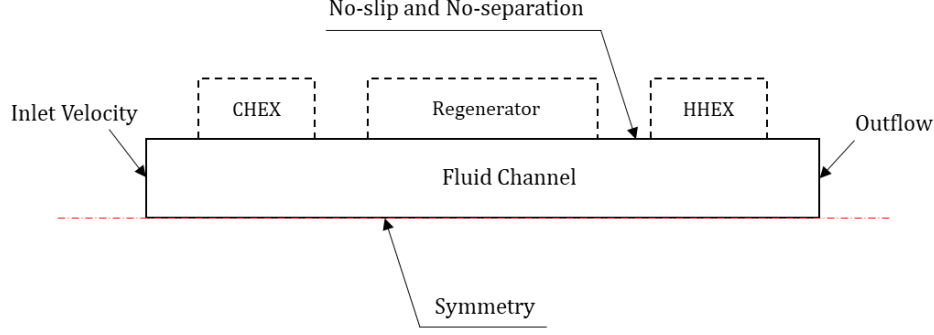
Fig. 3 Boundary conditions for obtaining velocity distribution in the channel

$$\boldsymbol{q} = -k_{GdR}\boldsymbol{\nabla}T_{GdR} \tag{8}$$

$$\rho_f C_{pf}\left(\frac{\partial T_f}{\partial t} + (\boldsymbol{u_f}\cdot\boldsymbol{\nabla})T_f\right) = k_f\nabla^2 T_f \tag{9}$$

where k_{GdR} is the thermal conductivity of the GdR, T_{GdR} is the absolute local temperature in the GdR, ρ_f is the density of the heat transfer fluid, C_{pf} is the specific heat capacity, $\boldsymbol{u_f}$ is simply zero (during magnetization, the fluid remains stationary), k_f is the thermal conductivity of the fluid, and T_f is the absolute temperature of the fluid. This part of Step 2 will consider the fluid as stationary, as previously mentioned. Since we are assuming constant properties for the stationary heat transfer fluid, Eq. (9) becomes,

$$\frac{\partial T_f}{\partial t} = \frac{k_f}{\rho_f C_{pf}}\nabla^2 T_f \tag{10}$$

As we have assumed that the heat exchangers have reached a steady-state, the temperatures of the CHEX and HHEX are considered constant at the values T_C and T_H respectively, where T_C is the steady-state temperature achieved by the CHEX after 600 cycles and T_H is the temperature of the surroundings to which the heat is rejected. Since we are not interested in the interactions of the fluid with the heat exchangers, we will focus on the area around the regenerator and neglect the heat transfer between the fluid and the heat exchangers. At the interface of the solid GdR and the fluid, there exists perfect thermal contact, i.e.,

$$k_f\left.\frac{\partial T_f}{\partial y}\right|_{interface} = k_{GdR}\left.\frac{\partial T_{GdR}}{\partial y}\right|_{interface} \tag{11}$$

The next part of step 2 involves the modeling of the cold blow. Here, the fluid is assumed to be flowing due to the advancement of the piston at the CHEX side. The part of the fluid that gets heated due to the magnetization of the GdR is pushed towards the HHEX, finally rejecting heat into the surroundings. The velocity distribution obtained in Step 1 may be used in conjunction with Eq. (9) to obtain the fluid's temperature distribution. During the cold blow, the magnetized GdR continues exchanging heat with the fluid. The boundary conditions remain the same as discussed earlier.

2.3.3 Step 3: Demagnetization and hot blow

In this step, the GdR is demagnetized, that is, the externally applied magnetic field is dropped to zero (in a single step). Assuming no hysteresis, the GdR loses its magnetization, which leads to a decrease in its internal energy. A decrease in internal energy translates to a reduction in the temperature of the GdR when compared to its temperature at the end of step 2. As in Step

2, we assume an adiabatic demagnetization of the regenerator. Therefore, Eq. (6) can be used here as well:

$$T = T_i^{II} + \Delta T_{\text{ad}}^{demag} \left(T_i', H_0\right) \tag{12}$$

where T_i^{II} is the temperature of the GdR at the end of Step 2, and $\Delta T_{\text{ad}}^{demag}$ is the adiabatic temperature change produced by switching off the external magnetic field H_0. Though Eq. (12) appears to be similar to Eq. (6), it is essential to note the difference in the initial temperatures used for each of the equations. After demagnetization, as the temperature of the GdR reduces to a value below the temperature of the fluid in its contact, it absorbs heat from the fluid, thereby cooling it. We assume that the heat transfer fluid and the regenerator interact only after the regenerator is completely demagnetized. In this way, the modeling of Step 3 becomes quite similar to that of Step 2 and Eqs. (7)-(11) may be conveniently used.

The distinction between Steps 2 and 3 arises when considering the modeling of the hot blow. In this part, the piston at the HHEX side is pushed towards the CHEX, which drives the cooled fluid section towards the CHEX. Finally, in the CHEX, the cool heat transfer fluid absorbs the cooling load from the target area. The completion of Step 3 concludes a single AMR cycle. Due to short piston stroke times, the AMR cycle has to be repeated multiple times to reach a no-load condition where the CHEX and the target area are in thermal equilibrium. As the target area releases more heat and disturbs the equilibrium, the AMR cycle restarts, and the removal of cooling load resumes until a steady state is reached again. Fig. 4 illustrates all the boundary conditions required for modeling steady-state heat transfer in the system.

(a)

(b)
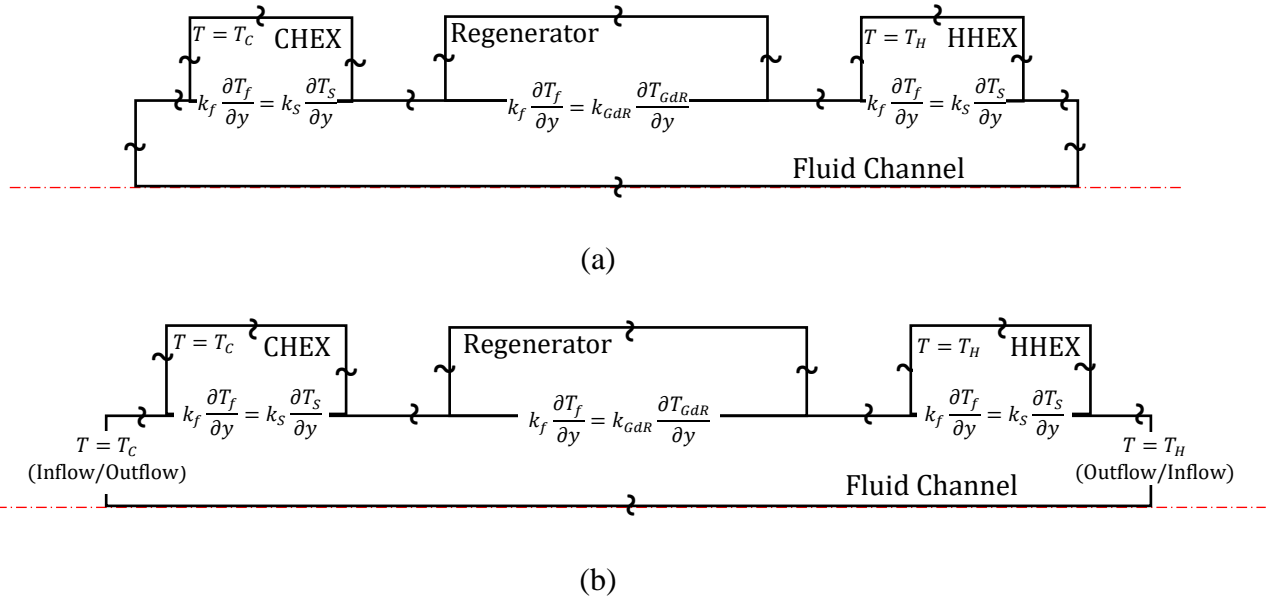
Fig. 4: Boundary conditions for heat transfer modeling: (a) Magnetization or demagnetization, (b) Cold or hot blow. Here the symbols $\sim$ and $\wr$ represent an adiabatic surface.

2.4 Material properties

Table 3 shows the material properties for all the components used in the model at 298 K [13]. Since our modeling procedure does not require the dynamic viscosities of the solid components, we have not mentioned them in Table 3. Though Table 3 provides us an estimate of the thermophysical properties of Gadolinium, it does not illustrate the dependence of its

properties on temperature and an externally imposed magnetic field. Petersen has proposed the WDS model to model the MCE of Gd [8]. From the formulations in [5,7,10,13], the equations required for obtaining the specific heat capacity, and the isothermal entropy change during magnetization of Gd (which may be used to obtain the adiabatic temperature change), can be numerically solved. Fig. 5 compiles the specific heat capacity and the adiabatic temperature change for Gd, obtained from the WDS model.
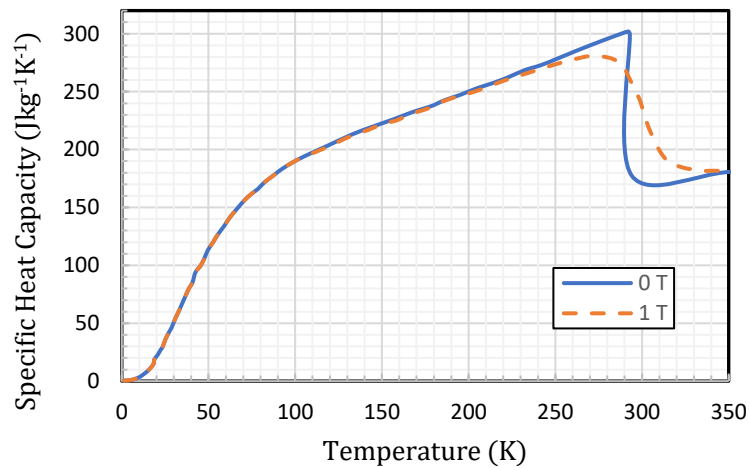
(a)
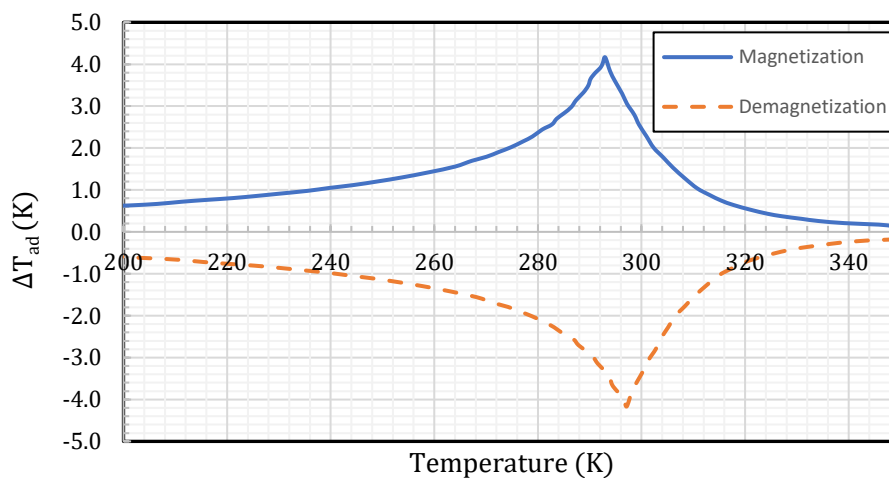
(b)

Fig. 5: Properties of Gd obtained from the WDS model: (a) Specific heat capacity during magnetization and demagnetization, (b) Adiabatic temperature change, as functions of temperature.

3. Results and discussion

3.1 Numerical model

The momentum and energy equations have been coupled and solved using the fully-coupled PARDISO solver built in the commercial software COMSOL Multiphysics 5.4. The application of this software for simulating an AMR process has been approved in several studies [7,8,14]. The Finite Element Method (FEM) incorporating Adaptive mesh refinement
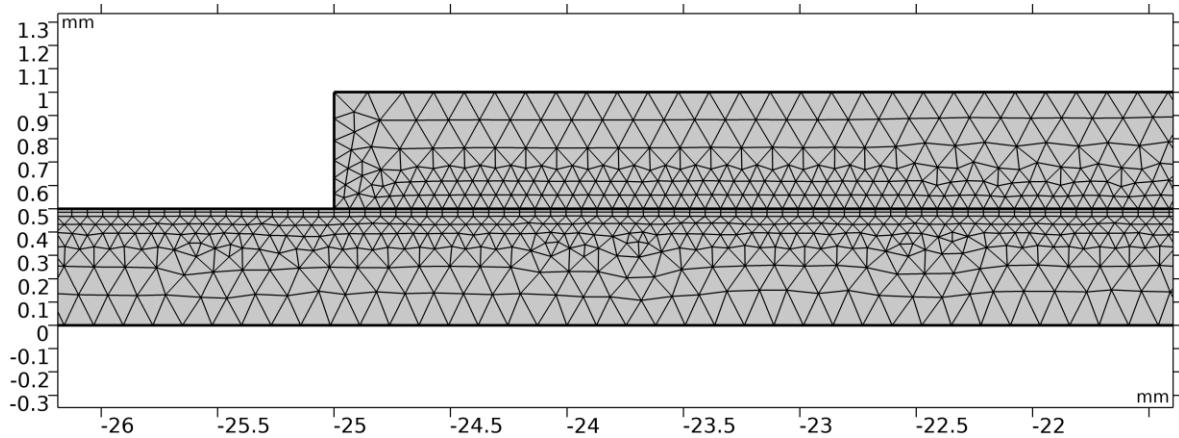
Fig. 6: A section of the generated mesh
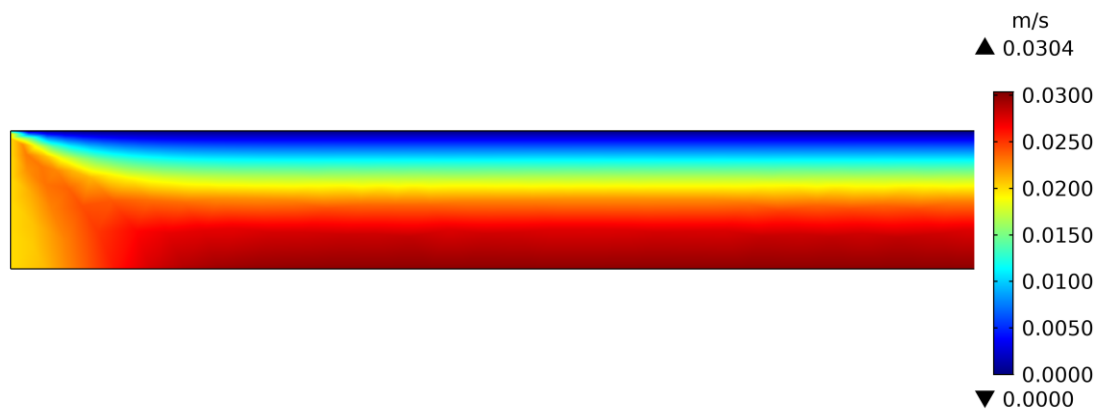
Fig. 7: Velocity distribution in the fluid half-channel

and error control has been employed in this work. There are 41516 triangular elements, and 4409 quadrilateral boundary elements in the mesh, which consists of 45925 elements in total. It has been found that for solving equations at the boundaries, quadrilateral elements give better accuracy than triangular elements [15]. Special attention has been provided to the proper resolution of boundary phenomena on the channel's surface by considering this point. Fig. 6 shows a section of the generated mesh. Since the aspect ratio of the channel is high, for visual clarity, the model is scaled down to 1/8 of the original size in the x-direction. The y-direction is scaled to 8 times the original height. A system with 3.47 GB usable RAM, an AMD A6-7310 APU processor with a clock frequency of 2.00 GHz has been used for solving the system of non-linear equations.

3.2 Velocity distribution

Fig. 7 demonstrates the velocity distribution in the fluid channel. The velocity field obtained, as expected, is typical of a standard channel flow. The maximum velocity in the system is $0.0304\ m/s$ which is higher than the fluid inlet velocity ($0.02\ m/s$). This is an effect of boundary layer formation in the fluid channel, per the principle of mass continuity. We have used the "laminar flow" physics interface of the software for modeling the hydrodynamic flow in the channel. However, we are yet to verify if the velocity results obtained from the simulation comply with the assumption of a perfect laminar flow in the channel. To do this, we calculate the Reynolds' number in the channel, using the maximum velocity. Due to the symmetry boundary condition, it is easy to deduce that the maximum velocity obtained for the half-

channel would be the same as the maximum velocity obtained in the complete full channel. For computing the Reynolds' number, we first define the hydraulic diameter of the channel as:

$$D_h = \frac{4A_c}{P} \tag{13}$$

where A_c is the cross-sectional area, and P is the wetted perimeter of the channel. Now, the Reynolds' number, based on the maximum velocity in the channel, may be obtained as:

$$Re_{D_h} = \frac{\rho v_{max} D_h}{\mu} \tag{14}$$

If the properties of water are obtained at 300 K, the Reynolds' number thus obtained is 34. This confirms that the assumption of laminar flow in the AMR system is valid.

Section 2 dictates that the fluid in the channel is stationary for $0 \le t \le 2\ s$. During the cold blow, the fluid enters the inlet near the CHEX at $t = 2\ s$, and the flow is maintained for a second. A similar situation occurs during demagnetization and hot blow, with the fluid entering from the HHEX side in the latter. Therefore, the system experiences a periodic inlet velocity boundary condition at both open ends of the fluid channel. To model this effect, we construct a step function for the inlet velocity, based on the sub-cycle times provided in Table 2. Since the sudden ramping-up of the inlet velocity may cause convergence problems in the solution, a second-order continuous derivative smoothing was applied to the inlet velocity profile.

3.3 Temperature distribution and span

For gauging the thermal performance of the AMR system, an accurate understanding of its temperature distribution is essential. This section discusses the temperature surface contours obtained from the simulation in two stages: Magnetization and cold blow, and demagnetization and hot blow.

3.3.1 Magnetization and cold blow

Fig. 8(a) illustrates the initial temperature distribution of the system. In the present study, the initial condition implies the instant when the magnetization process in the GdR is complete. It is assumed that before magnetization, there are no thermal gradients inside the GdR. For the sake of simplicity in modeling, we also assume that each point in the GdR experiences the exact same external magnetic field. Since the ΔT_{ad}^m at a point is dependent only on the local temperature before magnetization and the magnetic field (see Eq. (6)), one may say that after magnetization, all points in the GdR will have identical temperatures. However, this might not be precisely true. Since the model assumes perfect thermal contact at the domain interfaces, the boundary between the GdR and the fluid channel must agree on a common temperature. A similar situation exists for the heat exchangers. This is aptly described in Fig. 8(a). The color legend also shows the values for the maximum and minimum temperatures in the system. All temperatures are recorded in K.

As per discussion in the previous sections, we assumed that the MCE operates instantaneously, and the rest of the cycle time is allowed for heat transfer between the solid and the fluid domains. Since we start the cycle's $t = 0$ at the instant when magnetization is complete, the next two seconds of the cycle are spent in the heat transfer between the regenerator, heat exchangers, and the heat transfer fluid. This introduces temperature gradients in the otherwise isothermal domains. This phenomenon is demonstrated in Fig. 8(b), where the section of fluid near the regenerator is heated due to its magnetization. The hot fluid is then pushed towards the HHEX by the piston near the CHEX. The hot fluid, on entering the HHEX, finally loses
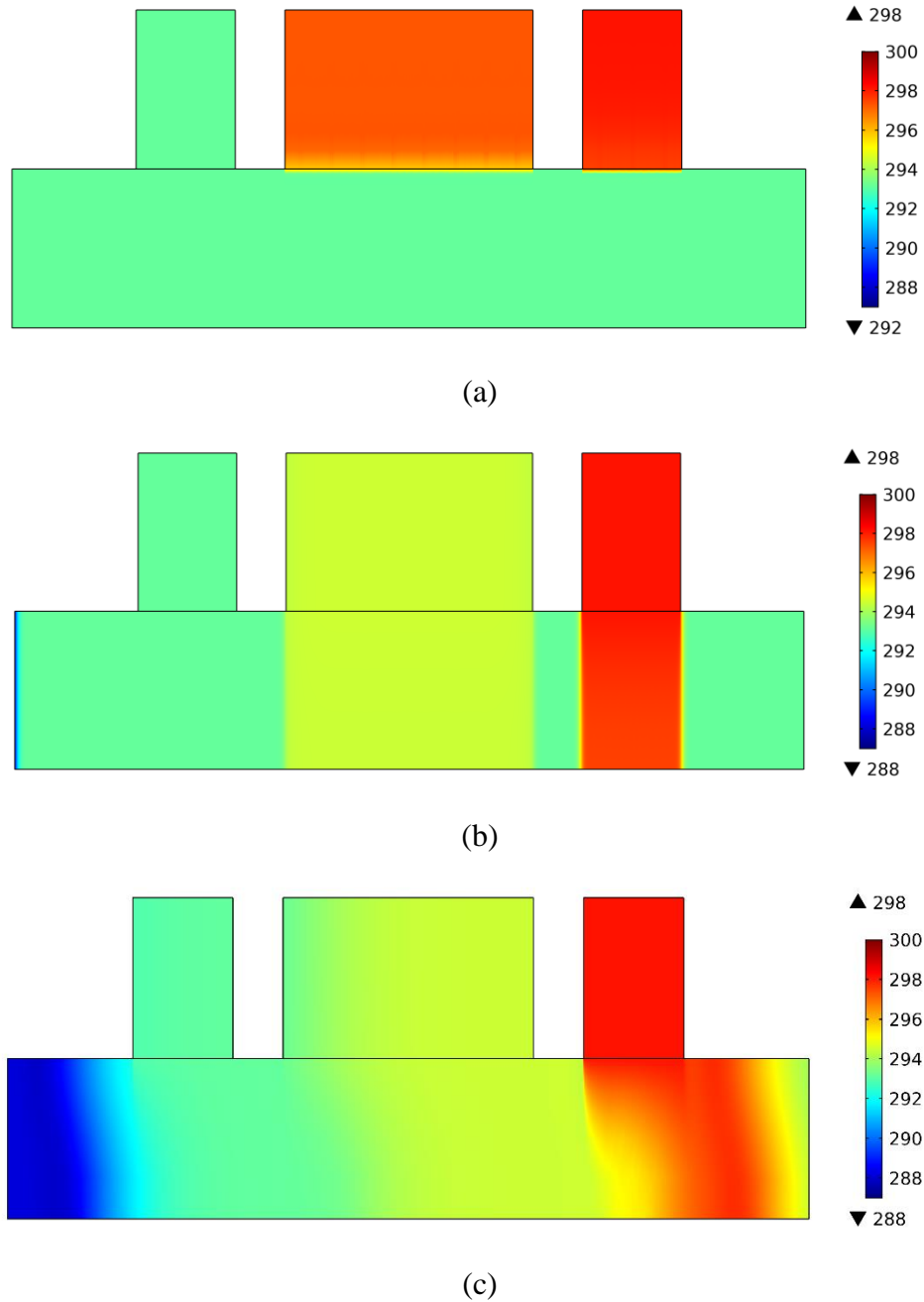
Fig. 8: Temperature distribution in the system (a) immediately after magnetization ($t = 0$) (b) just before cold blow ($t = 1.9\ s$) (c) immediately after cold blow ($t = 3.0\ s$)

heat to the surroundings, thereby cooling the fluid. Further, it can be observed that the cool fluid in the CHEX is being pushed towards the GdR to undergo a similar process in later cycles. The cold blow in the AMR cycle is shown in Fig. 8(c). The temperature of the surroundings is assumed to be 298 K. The temperature of the HHEX stays infinitesimally greater than the surroundings, ensuring reversible heat exchange between them.

3.3.2 Demagnetization and hot blow

Fig 9(c) illustrates the temperature distribution in the AMR system immediately after the cold blow. Clearly, the GdR is at a non-uniform temperature. It is at this moment, $t = 3.0\ s$, that the external magnetic field is switched off. Since hysteresis is neglected in the current study, the GdR is supposed to return to its initial state (the state before magnetization) as soon as the:
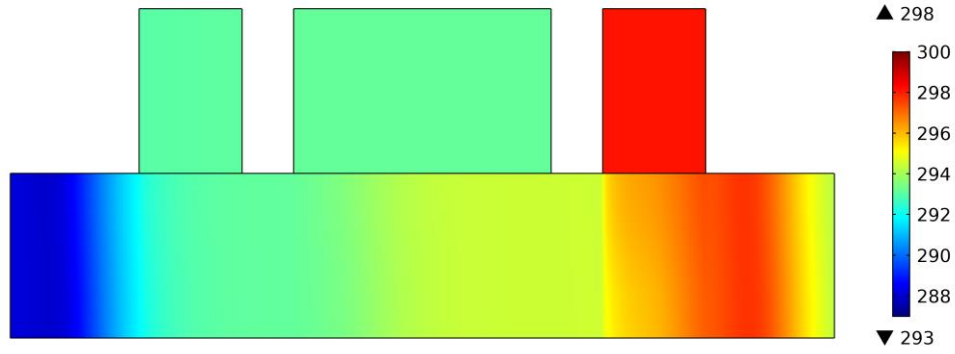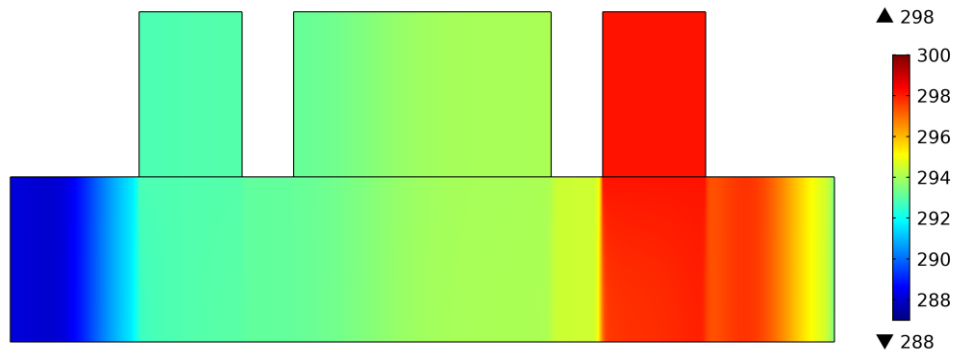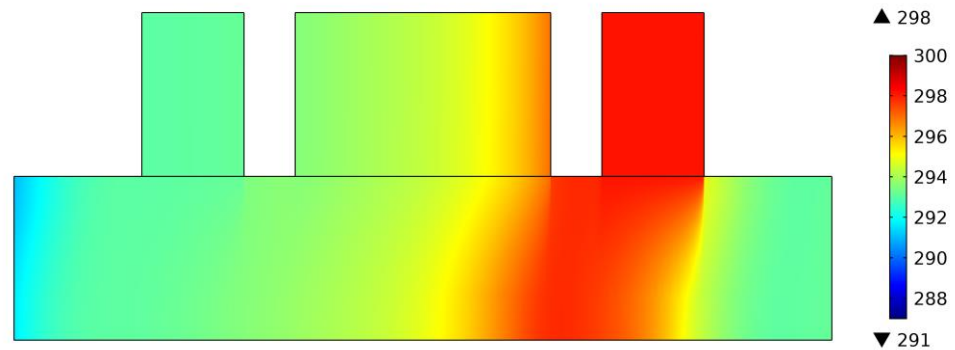
Fig. 9: Temperature distribution in the system (a) after demagnetization and settling ($t = 3.3\ s$) (b) just before hot blow ($t = 4.9\ s$) (c) immediately after hot blow ($t = 6.3\ s$)

magnetic field is removed. A decrease of ΔT_{ad}^{demag} is observed in the local temperature at all points of the GdR. This adiabatic temperature change depends on the state of the system immediately after the cold blow ($t = 3.0\ s$). A settling time of $0.3\ s$ is also provided to uniformize the temperature distribution in the system, as shown in Fig. 9(a). Starting at $t = 3.3\ s$, the GdR is allowed to absorb heat from the heat transfer fluid, thereby cooling the fluid. This is perhaps, one of the most important steps in the system, where the AMR is being prepared for removing heat from the target area. This step is illustrated in Fig. 9(b).

After the fluid section near the GdR is cooled for $2\ s$, the hot blow is executed. In the hot blow, as previously discussed, the piston on the HHEX side is pushed towards the CHEX, displacing

the cooled fluid section towards the CHEX. This enables the relatively "cool" fluid to absorb heat from the heat transfer fluid in the CHEX, further lowering the temperature of the CHEX, and allowing it to absorb the cooling load from the target area. The ultimate effect of the two steps mentioned in this section is the removal of heat from the target area. Therefore, an AMR cycle can be a potential replacement for the conventional vapor-compression cycles used in refrigeration and air-conditioning. However, AMR cycles have not been popularized as commercially viable technologies, which owes to several factors, for example, the use of rare-earth elements like Gadolinium and the limited temperature span obtained from the cycle.

Temperature span is an important aspect of any air-conditioning device that also governs the temperature ranges at which the device could be operated. Several definitions for temperature span have been proposed in HVAC literature. For the AMR cycle, we define ΔT, the temperature span, as

$$\Delta T = T_H - \bar{T}_C \qquad (15)$$

where T_H is the temperature of the HHEX, and $\bar{T}_c$ is the average surface temperature of the CHEX, which equals 288 K in this study. From the temperature distributions in Figs. 8 and 9, it is clear that the temperature span of the system considered in this study is ~10 K, which might just be sufficient for air-conditioning operations in an area with a mean temperature of 298 K. Under similar operating conditions, this also conforms to the value of temperature span reported by Petersen [8].

4. Conclusions

In this study, we have simulated a 2D CFD model of an AMR cycle using COMSOL Multiphysics 5.4. An AMR cycle has the potential to replace, at least partially, the conventional environment "unfriendly" vapor-compression cycles, for fulfilling refrigeration and air-conditioning requirements. The AMR cycle works on the principle of entropy transformation due to magnetization. The current model uses a Gadolinium regenerator for obtaining the desired refrigeration effects. First, we walk through the essentials of an AMR cycle and its functioning. Thereafter, we write the governing equations and the boundary conditions required for the solution of the former. We then obtain the temperature distributions for the system at different time instants, each of which is related to a crucial process occurring in the system. The trends observed in the contours were also explained in detail. Finally, we compute the maximum temperature span observed in the system throughout the AMR cycle and suggest that the current system might be feasible to employ in an air-conditioner's working cycle. This area can be further explored for applications to electric vehicles. For example, separate batteries to operate the pistons and permanent magnets for generating the external magnetic field could be used in a battery electric vehicle for air-conditioning [14].

5. References

[1]   Fraunhofer-Gesellschaft, Efficient heating for electric cars, Phys.Org. (2015). https://phys.org/news/2015-09-efficient-electric-cars.html?loadCommentsForm=1.

[2]   J. Voelcker, How Do Electric Cars (Volt, Leaf) Heat Passengers?, Green Car Reports. (2011). https://www.greencarreports.com/news/1054000_question-how-do-electric-cars-volt-leaf-heat-passengers.

[3]   XERIC, Innovative Climate-Control System to Extend Range of Electric Vehicles and Improve Comfort, 2015.

[4]   B. Sicre, P. Baumann, High-efficiency ventilation and heating systems by means of

solar air collectors for industry building refurbishment, Int. J. Low-Carbon Technol. 10 (2015) 139–145. https://doi.org/10.1093/ijlct/ctv002.

[5] J.A. Barclay, THEORY OF AN ACTIVE MAGNETIC REGENERATIVE REFRIGERATOR., in: NASA Conf. Publ., 1983: pp. 375–387.

[6] A.M. Tishin, Y.I. Spichkin, The magnetocaloric effect and its applications, IOP Publishing Ltd, Bristol, 2016. https://doi.org/10.1887/0750309229.

[7] T.F. Petersen, N. Pryds, A. Smith, J. Hattel, H. Schmidt, H.-J. Høgaard Knudsen, Two-dimensional mathematical model of a reciprocating room-temperature Active Magnetic Regenerator, Int. J. Refrig. 31 (2008) 432–443. https://doi.org/10.1016/j.ijrefrig.2007.07.009.

[8] T.F. Petersen, Numerical modelling and analysis of a room temperature magnetic refrigeration system, Tekniske Universitet, 2007.

[9] J.A. Barclay, S. Sarangi, SELECTION OF REGENERATOR GEOMETRY FOR MAGNETIC REFRIGERATOR APPLICATIONS., in: Am. Soc. Mech. Eng., American Society of Mechanical Engineers, 1984: pp. 51–58.

[10] KK. Nielsen, J. Tusek, K. Engelbrecht, S. Schopfer, A. Kitanovski, C.R.H. Bahl, A. Smith, N. Pryds, A. Poredos, Review on numerical modeling of active magnetic regenerators for room temperature applications, Int. J. Refrig. 34 (2011) 603–616. https://doi.org/10.1016/j.ijrefrig.2010.12.026.

[11] C. Aprea, A. Greco, A. Maiorino, C. Masselli, A comparison between rare earth and transition metals working as magnetic materials in an AMR refrigerator in the room temperature range, Appl. Therm. Eng. 91 (2015) 767–777. https://doi.org/10.1016/j.applthermaleng.2015.08.083.

[12] E. Schroeder, G. Green, J. Chafe, Performance predictions of a magnetocaloric refrigerator using a finite element model, 1990.

[13] D. Lide, CRC Handbook of Chemistry and Physics, CRC Press, 2004.

[14] A. Noume, M. Risser, C. Vasile, Modeling of a Magnetocaloric System for Electric Vehicles, in: 2013 COMSOL Conf. Rotterdam, 1998: pp. 1–6.

[15] R. V. Garimella, M.S. Shephard, Boundary layer mesh generation for viscous flow simulations, Int. J. Numer. Methods Eng. 49 (2000) 193–218. https://doi.org/10.1002/1097-0207(20000910/20)49:1/2<193::AID-NME929>3.0.CO;2-R.